

Neptunium^V Retention by Siderite under Anoxic Conditions: Precipitation of NpO₂-Like Nanoparticles and of Np^{IV} Pentacarbonate

Andreas C. Scheinost,^{*,†,‡} Robin Steudtner,[†] René Hübner,[§] Stephan Weiss,[†] and Frank Bok[†]

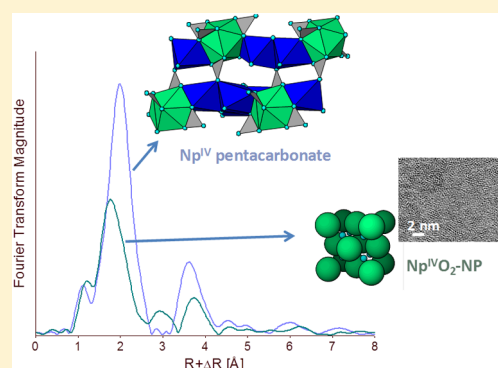
[†]Institute of Resource Ecology, Helmholtz-Zentrum Dresden - Rossendorf, D-01314, Germany

[‡]The Rossendorf Beamline at ESRF, F-38043 Grenoble, France

[§]Institute of Ion Beam Physics and Materials Research, Helmholtz-Zentrum Dresden - Rossendorf, D-01314, Germany

Supporting Information

ABSTRACT: The Np^V retention by siderite, an Fe^{II} carbonate mineral with relevance for the near-field of high-level radioactive waste repositories, was investigated under anoxic conditions. Batch sorption experiments show that siderite has a high affinity for aqueous Np^VO₂⁺ across pH 7 to 13 as expressed by solid-water distribution coefficients, $\log R_d > 5$, similar to the $\log R_d$ determined for the (solely) tetravalent actinide Th on calcite, suggesting reduction of Np^V to Np^{IV} by siderite. Np L₃-edge X-ray absorption near edge (XANES) spectroscopy conducted in a pH range typical for siderite-containing host rocks (7–8), confirmed the tetravalent Np oxidation state. Extended X-ray absorption fine-structure (EXAFS) spectroscopy revealed a local structure in line with NpO₂-like nanoparticles with diameter < 1 nm, a result further corroborated by high-resolution transmission electron microscopy (HRTEM). The low solubility of these NpO₂-like nanoparticles ($\sim 10^{-9}$ M), along with their negligible surface charge at neutral pH conditions which favors particle aggregation, suggest an efficient retention of Np in the near-field of radioactive waste repositories. When Np^V was added to ferrous carbonate solution, the subsequent precipitation of siderite did not lead to a structural incorporation of Np^{IV} by siderite, but caused precipitation of a Np^{IV} pentacarbonate phase.



INTRODUCTION

Nuclear power generation has left behind a legacy of high-level radioactive waste, which needs to be kept safe for hundreds of thousands of years. The disposal of this waste in deep geological formations behind multiple barriers is a concept favored by many nuclear power producing countries to ensure a lasting protection of people and the environment. The multiple barrier system consists of three principal parts, an engineered barrier (copper or stainless steel containers), a geo-engineered barrier (cement or clay-based backfill-material, e.g. bentonite), and the geological barrier (argillaceous, granitic or salt host rock).¹ Many of these components contain or form Fe^{II}-bearing minerals, which may act as scavenger for potentially released radionuclides by their reducing power and sorption capacity. Steel containers are likely to corrode under near-field conditions, forming for instance magnetite, siderite, chukanovite and Fe-phyllsilicates in contact with clay backfill,^{2,3} magnetite and hydrous Fe^{II} oxides in contact with brine,⁴ and Fe^{II} sulfides in the presence of sulfate reducing bacteria.⁵ Such Fe^{II}-bearing minerals also occur naturally in clay rocks; for example, MX80 bentonite considered as backfill material contains 0.7% siderite and 0.3% pyrite, and Opalinus clay considered as host rock in Switzerland contains 6% siderite and 0.9% pyrite.^{6,7}

Spent nuclear fuel consists mainly of the original uranium dioxide ($\sim 95\%$) and its fission products (lanthanides, technetium, selenium, noble gases, and cesium, $\sim 4\%$). Neutron absorption and decay reactions lead to the formation of plutonium ($\sim 1\%$) and the minor actinides neptunium, americium and curium ($< 0.1\%$ of typical burnt fuel). The redox-sensitive elements uranium, plutonium, technetium, selenium have been shown to be efficiently immobilized by sorption and redox reactions on Fe^{II}-bearing minerals.^{4,8–14} Much less work has been conducted on the redox-driven (anoxic) immobilization of the minor actinide neptunium, although its major radionuclide ²³⁷Np has a very long half-life (2.14 Mio years) and contributes significantly to the long-term radiotoxicity of spent fuel. Work attempting to elucidate the mechanisms of Np reduction by mineral surfaces is even more scarce. Np^V was found to be much more strongly retained by magnetite under anoxic conditions than under atmospheric conditions; using a liquid extraction technique, Np associated with the solid phase was determined to be tetravalent.¹⁵ In

Received: May 17, 2016

Revised: September 1, 2016

Accepted: September 2, 2016

Published: September 2, 2016

comparison to reduction by aqueous Fe^{II} , reduction by magnetite was 3 orders of magnitude faster.¹⁶ A pioneering study employing EXAFS spectroscopy showed that Np^{V} was only weakly taken up by mackinawite, forming rather surprisingly a mononuclear Np^{IV} sorption complex coordinated to both O and S.¹⁷ In the presence of green rust, Np^{V} was rapidly sorbed and reduced to Np^{IV} at the edges of the hexagonal platelets; the authors suggest formation of Np^{IV} particles, but their identification by TEM remained elusive.¹⁸ Np^{V} reacted with Opalinus clay was reduced to Np^{IV} and showed a strong association with pyrite particles embedded in the clay matrix; the exact nature of the reduced Np^{IV} could not be identified, but the authors excluded formation of NpO_2 due to the absence of Np-Np backscattering contributions in $\text{Np L}_{3\text{-edge}}$ EXAFS spectra.¹⁹ Biotite and chlorite with structural Fe^{II} fully reduced Np^{V} to Np^{IV} , and nanoparticulate NpO_2 formed as identified by EXAFS.²⁰ In the presence of Ti-doped magnetite, sorption of Np was high at pH values 5 and 7, while the sorption at pH 3 was low, but increased with Ti-doping most likely because of the increasing Fe^{II} fraction to counterbalance the charge of structural Ti^{IV} . Using $\text{Np L}_{3\text{-edge}}$ XANES and EXAFS, the reaction product could be identified as a Np^{IV} species, while the absence of Np-Np backscattering contradicted formation of NpO_2 .²¹ The authors claim formation of an inner-sphere sorption complex, but fitted Np-Fe and Np-Ti coordination numbers between 5 and 7 would rather suggest structural incorporation by magnetite or a secondary Fe phase. In conclusion, the few studies on Np uptake by Fe^{II} -bearing minerals under anoxic conditions show sorption and reduction to Np^{IV} , but the reaction mechanism and the end product, that is, sorption complexation vs structural incorporation vs NpO_2 precipitation, often remain elusive.

The objective of our study was therefore, to investigate the Np reduction products on siderite under strictly anoxic atmosphere by $\text{Np L}_{3\text{-edge}}$ XANES and EXAFS spectroscopy and electron microscopy. The Fe^{II} carbonate siderite was selected because of its relevance for many high-level radioactive waste scenarios as outlined above. In comparison to other Fe^{II} -bearing phases like green rust, magnetite and mackinawite, the electron transfer provided by siderite (or by the hydroxocarbonate chukanovite) generally seems to be smaller, as revealed by a lesser amount of reduction, smaller reduction kinetics, or reduction not to the lowest possible but to an intermediate oxidation state only. This has been demonstrated for instance for uranium, plutonium, and selenium.^{11,22–24} A reason for this is certainly the larger electronic bandgap of siderite as compared to green rust, magnetite and mackinawite with their almost metal-like electron conduction, which strongly limits the supply of electrons from the mineral structure to adsorbed (metal) oxidants.²⁴ An additional reason might be that dissolved carbonate forms complexes with Fe^{II} and potentially also with the metal oxidant, thereby competing with the Fe/oxidant redox reaction.^{11,22–26} Therefore, the purpose of our study was to investigate, whether or not Np^{V} is reduced by siderite, to characterize the oxidation state and local structure of the reaction product and to decipher, if possible, the reaction pathway.

MATERIALS AND METHODS

Caution! ^{237}Np is a radioactive isotope and an α -emitter. It should be handled in dedicated facilities with appropriate

equipment for radioactive materials to avoid health risks caused by radiation exposure.

Generally, all sample manipulations, including mineral synthesis and washing, UV-vis measurements, and preparation of samples for XAS measurements, were carried out under anoxic conditions in a nitrogen glovebox with 0–5 ppmv O_2 . Experiments were carried out at RT (23 ± 3 °C); deionized (18.2 M Ω cm Milli-Q), degassed (O_2 and CO_2 free) water was used for all purposes. Eh measurements were performed by dipping a conventional ORP (oxidation–reduction potential) electrode with platinum disc (Sentix, WTW) in the unstirred suspensions. pH measurements were performed with glass electrodes with 3 M KCl (Sentix Micro, WTW) calibrated against standard pH buffers. No ionic strength correction was done for measurements at $I = 1.0$ M NaCl. According to Felmy et al. the estimated difference between pH_{exp} and pH_c ($= -\log[\text{H}^+]$) is smaller than 0.15 pH units.²⁷

Siderite Synthesis and Characterization. A siderite ($\text{Fe}^{\text{II}}\text{CO}_3$) suspension ($[\text{Fe}_{\text{tot}}] = 0.2$ M) was prepared by slowly mixing 100 mL of a 0.4 M $\text{Fe}^{\text{II}}\text{Cl}_2$ solution with 100 mL of a 0.8 M Na_2CO_3 solution.²⁸ The light gray precipitate was washed with 0.1 M NaCl (at least 3 washing cycles) and kept in suspension in 0.1 M NaCl. Siderite is extremely oxidation-sensitive and not stable in suspension with an ionic strength (I) lower than 0.1 M, as indicated by the rapid appearance of brownish Fe^{III} oxyhydroxides like goethite.^{29,30} Raman spectroscopic measurements were carried out with a Raman-microscope (HORIBA Jobin Yvon LabRAM Aramis Vis) using an argon-ion laser (437 nm) with an output energy of 0.2 mW as light source and confirmed the phase identity and purity of the siderite stock suspension (see Figure S1 in the Supporting Information (SI)). An isoelectric point of 10.1 was determined by zeta potential measurements using a laser-doppler-electrophoresis instrument (Zetasizer nano-ZS, Malvern Instruments Ltd.) (SI Figure S2).

Np^{V} Stock solution. A 0.056 M Np^{VI} stock solution in 1.0 M HClO_4 was prepared from neptunium (^{237}Np) dioxide (CEA-Marcoule, France), according to a previously reported procedure.³¹ The pentavalent oxidation state of Np was prepared by electrochemical reduction from Np^{VI} and verified by UV-vis-NIR spectroscopy. This solution was diluted with degassed deionized water to obtain a stock solution of 10^{-3} M Np^{V} used for the sorption experiments.

Np Sorption on Siderite. The Np^{V} retention by siderite was investigated in the pH range 7 to 13 by batch experiments. For pre-equilibration, siderite suspensions (S/L ratio of 1 g/L) were prepared in either 0.1 M NaCl or 0.1 M Na_2CO_3 background electrolyte ($V = 10$ mL) and continuously shaken on a horizontal shaker for 48 h, with pH values initially adjusted and readjusted if necessary. Then, aliquots of the Np^{V} stock solution were added to the siderite suspensions to obtain the final Np^{V} concentration of $2 \cdot 10^{-5}$ M. The pH values were readjusted immediately by addition of NaOH or HCl. The samples were shaken up to 3 weeks, whereby the pH was monitored and readjusted if necessary. Finally, the remaining suspensions were centrifuged for phase separation (60 min, 3200g). The final Np concentration in the supernatant was determined by liquid scintillation counting (LSC, Winspectral α/β , Wallac 1414, Perkin-Elmer) using α/β discrimination with a lower detection limit $\leq 10^{-9}$ M. The distribution coefficient R_d in L/kg was calculated as follows

$$R_d = \frac{c_{\text{ini}} - c_{\text{eq}}}{c_{\text{eq}}} \cdot \frac{V}{m}$$

where c_{ini} and c_{eq} (mol/L) are the initial and equilibrium Np concentration in solution, V (L) the sample volume and m (kg) the mass of siderite. Note that the sorption conditions were chosen to obtain samples with sufficient Np concentration to be measured by EXAFS spectroscopy (see below).

Np Siderite Coprecipitation. In addition to the batch sorption experiments, where Np^{V} was added to presynthesized siderite, we also conducted a Np^{V} -siderite coprecipitation experiment at pH 10.5 to study the eventual structural incorporation of Np. This experiment was performed like the pure mineral synthesis described before, except that an appropriate aliquot of the Np stock solution to obtain a nominal Np loading on siderite of 4705 mg/kg was slowly added to the $\text{Fe}^{\text{II}}\text{Cl}_2$ solution, before adding the Na_2CO_3 solution to initiate the siderite precipitation. The sample was examined by XANES and EXAFS after a washing step with 0.1 M NaCl without any further aging.

X-ray Absorption Spectroscopy (XAS). We selected three different types of samples (see SI Table S1): (i) to investigate the influence of reaction time on sorption a time series collected after 1 hour, 1 day, 7 and 21 days, at pH 7.7 ± 0.3 , that is, in the pH range predominant in siderite-containing host rocks,^{6,7,32} and an ionic strength of 0.1 M; (ii) to investigate the influence of ionic strength on sorption two additional samples in 0.001 and 1 M NaCl background electrolyte at the same pH and after a reaction time of 7 days; (iii) to investigate the potential incorporation of Np by siderite the coprecipitation sample as described before. After phase separation by centrifugation, the solids were filled into double-confinement, heat-sealed polyethylene sample holders inside the anoxic glovebox. The samples were then removed from the glovebox and immediately flash-frozen in LN_2 and stored in an LN_2 dewar to prevent oxygen diffusion into the samples and to freeze-in chemical reactions until XAS measurements. After transport to the Rossendorf Beamline at ESRF (Grenoble, France), the samples were individually removed from the LN_2 dewar and transferred to a closed-cycle He cryostat operating at 10 K within less than 30 s for the XAS measurements. XAS (XANES and EXAFS) measurements were carried out in fluorescence mode at the Np- L_3 edge (17 610 eV) using a 13-element high-purity Ge solid state detector (Canberra) with digital signal analysis (XIA XMap). The polychromatic synchrotron beam was monochromatized using a pair of water-cooled Si(111) crystals, and higher-order harmonics were rejected by a Rh-coated 1.3-m long collimating mirror before the double-crystal monochromator, and a 1.2-m long Rh-coated toroidal mirror after the monochromator. Between 6 and 12 individual XAS scans were energy-calibrated against a simultaneously measured Y foil (17 038 eV), corrected for fluorescence deadtime and averaged using SIXpack, while subsequent data reduction steps and shell fits were conducted using WinXAS.^{33,34} Theoretical backscattering paths were calculated with FEFF8.2 using crystal structures of NpO_2 and siderite (with one Fe replaced by Np).^{35–37} Shell fits were performed with an amplitude reduction factor, S_0^2 , of 0.9 in the k -range 2.0 to 11.5 \AA^{-1} . Reference spectra for the Np^{IV} aquo complex³⁸ and for NpO_2 ³⁹ were downloaded from AcReDaS, the online actinide reference database for spectroscopy.⁴⁰

Transmission Electron Microscopy (TEM). A sample ($[\text{Np}^{\text{V}}]_{\text{ini}} = 2 \cdot 10^{-5}$ M, $S/L = 0.1$ $\text{g}\cdot\text{L}^{-1}$, $I = 0.1$ M (NaCl),

reacted for 7 days under anoxic conditions) was prepared by disposing a drop of the Np-siderite suspension on a carbon-coated copper grid (400 mesh, S 160, Plano GmbH) and drying it under inert gas atmosphere. Bright-field TEM and high-resolution TEM (HRTEM) images were collected on an image C_s -corrected Titan 80–300 electron microscope (FEI) operated at 300 kV. Reciprocal space diffractograms were derived from the HRTEM micrographs by Fast Fourier Transform (FFT) analysis. Energy-dispersive X-ray spectroscopy (EDXS) was performed in scanning TEM mode with a Li-drifted silicon detector (EDAX).

RESULTS AND DISCUSSION

The Np^{V} uptake by siderite during the sorption experiments is very high with $\log R_d$ values always above 5 and little variation across the pH range 7 to 13 (Figure 1 top). The addition of 0.1

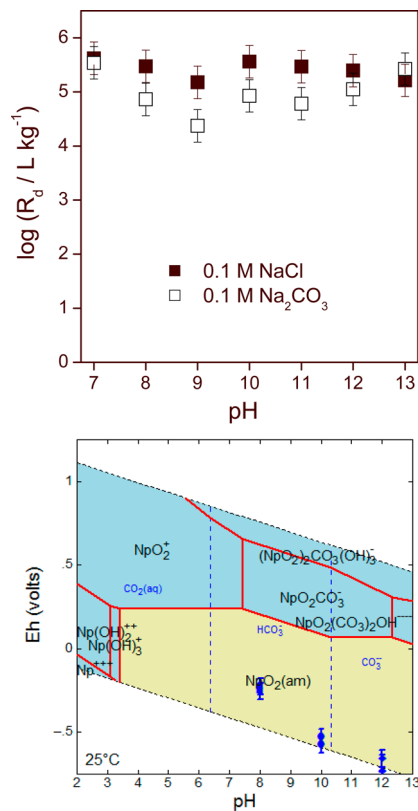


Figure 1. Top: Np solid/liquid distribution coefficient in the siderite system as function of pH. $[\text{Np}^{\text{V}}]_{\text{ini}} = 2 \cdot 10^{-5}$ M, $S/L = 1$ $\text{g}\cdot\text{L}^{-1}$, $I = 0.1$ M NaCl or NaCO_3 as indicated, after 1 week reaction time under anoxic N_2 . Bottom: Eh-pH diagram calculated for the chemical system $2 \cdot 10^{-5}$ M Np^{V} in 0.1 M NaCl solution in presence of siderite under anoxic conditions at 25 °C (carbonate activity determined by siderite solubility). Thermodynamic data of the Lawrence Livermore National Laboratory thermo database were supplemented by the most recent NEA database.^{44,45} Results of batch experiments are represented by blue symbols.

M carbonate reduced Np uptake significantly between pH 8 and 11, that is, in the pH region where siderite solubility is low (Figure S3). In comparison to the Np^{V} uptake by the (redox-inactive) Ca carbonate calcite, these $\log R_d$ values are 2–3 orders of magnitude higher,⁴¹ and much more similar to values obtained for the tetravalent actinide, Th, on calcite,⁴² in both cases at comparable pH. Hence the high R_d values are a first

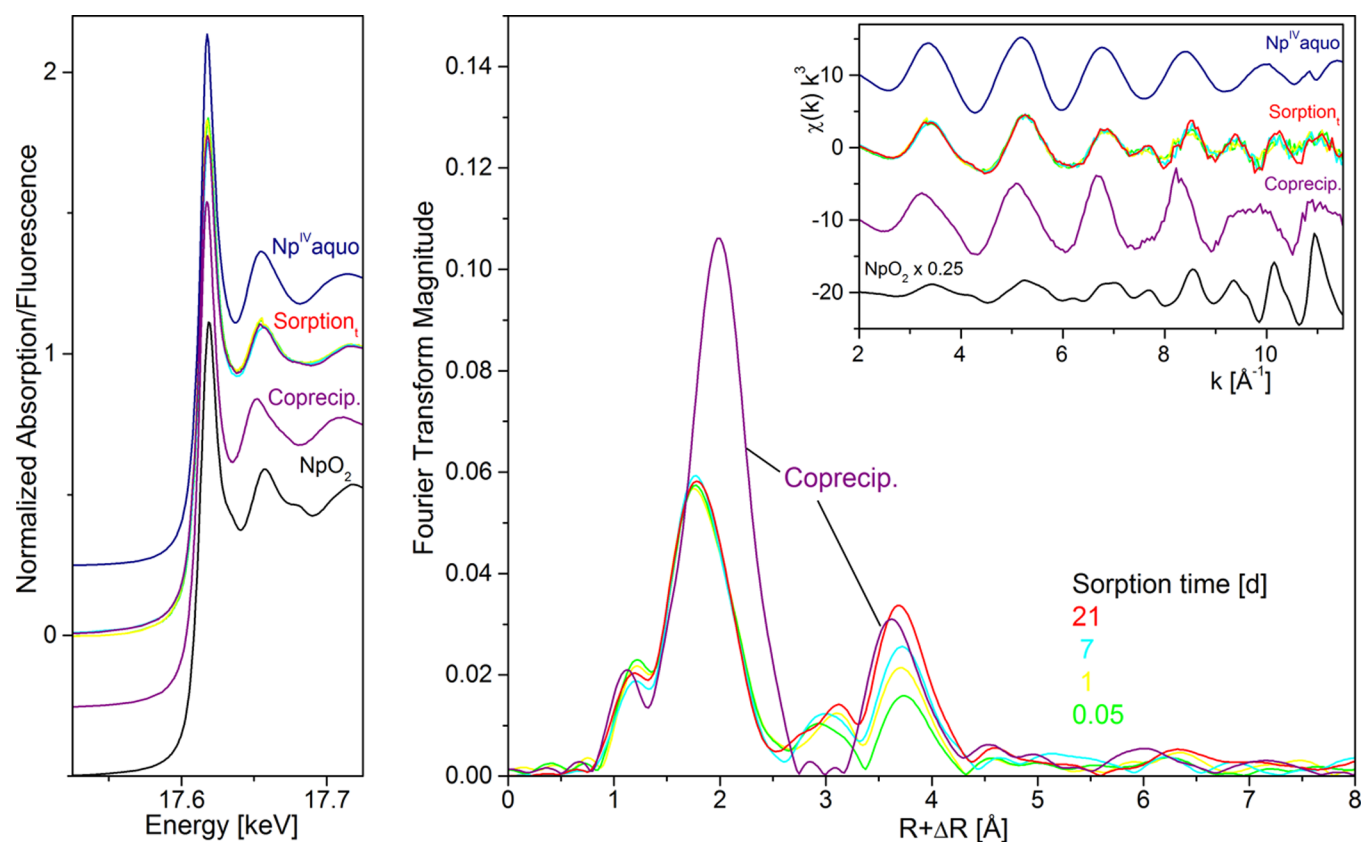


Figure 2. Neptunium L_3 -edge XAS spectra of selected siderite sorption and coprecipitation samples ($\text{pH } 7.7 \pm 0.3$) along with Np references. Left: XANES spectra, right: EXAFS Fourier transform magnitude and corresponding $\chi(k)$ spectra as insert.

Table 1. Np- L_3 XANES Edge Energies and EXAFS Fit Results of Np Siderite Samples and References.

sample	E_0 [eV]	first shell			second shell			ΔE_0 [eV]	$\chi^2_{\text{res}} \%$
		CN ^a	R^b [Å ²]	σ^{2c} [Å ²]	CN	R [Å]	σ [Å ²]		
sorp. 1 h (0.1 M)	17613.3	8.0 O	2.35	0.0100	2.1 Np	3.83	0.0026	7.1	19.3
sorp. 1 d (0.1 M)	17613.4	7.7 O	2.35	0.0100	4.4 Np	3.84	0.0100	7.6	19.8
sorp. 7 d (0.1 M)	17613.3	7.8 O	2.34	0.0100	3.9 Np	3.83	0.0054	7.4	16.4
sorp. 21 d (0.1 M)	17613.5	7.9 O	2.34	0.0100	3.8 Np	3.82	0.0034	7.0	13.8
sorp. 0.001 M (7 d)	17613.6	8.4 O	2.35	0.0100	3.4 Np	3.83	0.0027	7.4	14.6
sorp. 1 M (7 d)	17613.6	8.0 O	2.34	0.0100	3.6 Np	3.83	0.0060	7.3	15.5
coprecipitate	17613.8	9.6 O	2.41	0.0048	4.2 C _{bid}	2.87	0.0010	14.6	12.8
					4.2 ^d O _{dist}	4.14 ^d	0.0016 ^d		
					8.4 ^{2d} C _{bid} -O _{dist}	4.14 ^d	0.0016 ^d		
					4.2 ^d C _{bid} -O _{dist} -C _{bid}	4.14 ^d	0.0016 ^d		
Np ^{IV} aquo	17613.8	11.6 O	2.39	0.0083				9.4	5.2
NpO ₂	17613.6	8 O	2.35	0.0043	12 Np	3.85	0.0010	9.6	19.4
					24 O	4.48	0.0010		
NpO ₂ crystal structure ⁴⁷		8 O	2.35		12 Np	3.84			
					24 O	4.51			

^aCN: coordination number, error $\pm 25\%$. ^b R : Radial distance, error ± 0.01 Å. ^c σ^2 : Debye–Waller factor, error ± 0.0005 Å². ^dValues correlated during fit.

indication that Np^V was reduced to Np^{IV} by siderite. Further support comes from by the thermodynamic calculation, showing that the equilibrium should be dominated by NpO₂ at the Eh values measured at pH 8, 10, and 12 (Figure 1 bottom).

Figure 2 shows the Np- L_3 edge XANES spectra of the siderite sorption time series at $\text{pH } 7.7 \pm 0.3$, and of the coprecipitation sample. All spectra are well aligned and correspond both in edge and white-line position with the two

Np^{IV} references, NpO₂ and the Np^{IV} aquo complex.^{38,39} This is further confirmed by the XANES edge energies as determined by the knot of the second derivative, which vary by less than 0.3 eV from the average of 17 613.5 eV (Table 1). Furthermore, iterative transformation factor analysis performed with the software package ITFA on the XANES spectra revealed only one spectral component for the sorption samples, indicating that possible traces of Np^V remain below 5%.⁴³ Therefore, Np^V

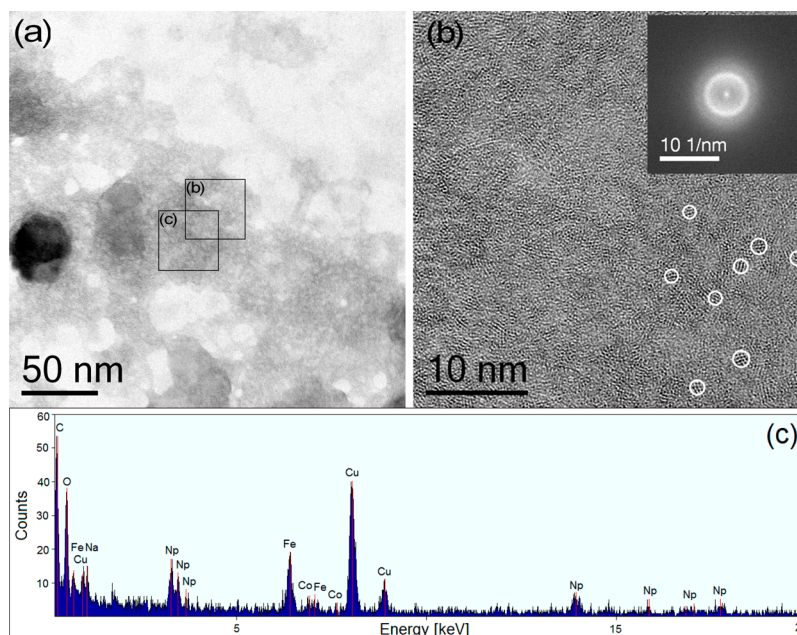


Figure 3. (a) Bright-field TEM micrograph of a 7-d sorption sample. (b) HRTEM image of area (b) with corresponding Fast Fourier Transform (FFT) in the inset. Some nanocrystals are marked by circles. (c) Energy-dispersive X-ray (EDX) spectrum obtained in scanning TEM mode from the area (c).

is reduced to Np^{IV} in all systems, even already after the shortest sorption time of 1 h, and also in the coprecipitation sample.

The EXAFS Fourier transform magnitudes of the sorption samples show a coordination shell at $R + \Delta R = 1.8 \text{ \AA}$ (uncorrected for phase shift), which is fitted by about 8 oxygen atoms at a distance of $2.34 - 2.35 \text{ \AA}$. Note that the small peak at the left side of this coordination shell cannot be fitted with a Np–O distance of 1.87 \AA as would be expected for the $-\text{yl}$ group of Np^{V} ; they constitute instead a truncation artifact of the Fourier transformation arising from the relatively short k -range. A second peak at $R + \Delta R = 3.7 \text{ \AA}$ increases in height with sorption time. Wavelet analysis of this peak reveals an amplitude maximum at $k > 10 \text{ \AA}^{-1}$, in line with backscattering by a heavy element.⁴⁶ Correspondingly, this shell could be fitted with Np atoms at a distance of $3.82 - 3.84 \text{ \AA}$ (see exemplary fit in Figure S4).

The interatomic distances (R) for these nearest Np–O and Np–Np shells are close to those of NpO_2 . This is also true for the coordination numbers (CN) of the Np–O coordination shell, which are close to 8 as in the cubic NpO_2 structure. In contrast, the CNs of the Np–Np path are much lower, and their Debye–Waller factors (σ^2) as measure of static disorder much larger, than those of NpO_2 , suggesting formation of nanoparticles.⁴⁷ Assuming NpO_2 particles with 1 nm diameter, one can calculate an average Np–Np coordination number of 5.5 ($12 \times 5 + 1 \times 12$) for the cluster containing 13 Np atoms. This coordination number is significantly higher than the ones derived from the EXAFS shell fit (3.5 per average for all sorption samples), suggesting an even smaller average particle size, or cation vacancies. Similar trends were observed for nanocrystalline Np dioxide particles formed after dilution of aqueous Np^{IV} carbonate complexes³⁹ and for other An^{IV} oxide/hydroxide species.^{48–50} Therefore, the EXAFS analysis suggests that Np^{V} reduction at the siderite surface leads to the formation of either small particles of crystalline NpO_2 or to structurally disordered Np^{IV} oxide/hydroxide. While the peak height of the Np–Np shell increases with increasing sorption time, suggesting

the growth of nanoparticles with time, the shell fit data suggest a more complicated process: between 1 hour and 1 day sorption time, the CN doubles from 2 to 4, but then remains constant. At the same time, the Debye–Waller factor increases from 0.0026 to 0.0100 \AA^2 , and decreases thereafter with increasing equilibration time to 0.0034 \AA^2 . This suggests that the initial particles are small, but well ordered, and then grow with high disorder, which subsequently obtain a higher degree of order with equilibration time. Ionic strength of the background electrolyte also shows a significant effect on the Debye–Waller factor, which increases from 0.0027 to 0.0054 to 0.0060 \AA^2 , when the ionic strength increases from 0.001 to 0.1 to 1 M for a constant reaction time of 7 days. Therefore, increasing background electrolyte concentrations increasingly interferes with the crystallization process.

To further characterize the microstructure of the Np^{IV} phase, a 7-d sorption sample was analyzed using TEM. A typical bright-field TEM micrograph is shown in Figure 3a. While the black particle with a diameter of approximately 40 nm is siderite, the gray areas arise from particles much smaller. The HRTEM micrograph (Figure 3b) shows periodic structures with diameters $\leq 1-2 \text{ nm}$ (marked by circles). The diffractogram based on Fast Fourier Transform (FFT) analysis of the HRTEM image consists of diffuse rings as expected for such nanocrystalline material, which are not accessible to structure analysis. However, the dominant presence of Np and O determined in an adjacent region by energy-dispersive X-ray (EDX) spectroscopy (Figure 3c) confirms that these small particles constitute indeed the Np phase (Note that C and Cu contributions stem from the TEM support grid, and Fe and Co from the objective lens pole piece). Extended electron irradiation (1–2 min.) induced particle growth, and the FFT-derived diffractograms produced now distinctive rings in agreement with the fluorite-type NpO_2 structure ($Fm\bar{3}m$) (SI Figure S5).⁵¹ Thus, the TEM-derived particle size of the unaltered material and the phase identification after the electron-induced particle growth support the EXAFS analysis

that Np^{IV} is precipitated as NpO_2 or a hydrated precursor phase with particle sizes around 1 nm or even smaller.

In contrast to the sorption samples, the EXAFS Fourier transform magnitude of the coprecipitation sample shows a much higher and more distant coordination shell (Figure 2 right), which could be fitted with ~ 10 oxygen atoms at a distance of 2.41 Å, that is, not commensurate to the cubic NpO_2 structure (Table 1). Furthermore, the second shell is at a shorter distance than the Np-Np shell of NpO_2 . Wavelet analysis of this shell shows a maximum of k at about 8 \AA^{-1} , and hence discards that this peak arises from Np-Np backscattering. The spectrum is in fact similar to compounds where carbon is bidentately coordinated, like in Ce^{IV} or U^{IV} carbonate compounds.⁵² This was confirmed by a shell fit based on this bidentate arrangement, which gives rise to very characteristic multiple scattering paths involving the nearest bidentately coordinated C (C_{bid}) and the next nearest, distal O (O_{dist}) atom of the carbonate molecule. The Np-O coordination number of ~ 10 as well as the Np- C_{bid} coordination number of 4.2 (theoretically 5) confirm the formation of $\text{Np}^{\text{IV}}(\text{CO}_3)_5$ units very similar to those found for U^{IV} and Pu^{IV} before, in line with the similar complex formation constants of all three actinides.^{45,52,53} As expected for the slightly smaller ionic radius of Np^{IV} versus U^{IV} , the fitted radial distances are about 0.02 Å shorter than for the U^{IV} carbonate unit (Table 1). Analogous to U^{IV} , the Np^{IV} pentacarbonate unit may exist either as aquo-anion complex,³⁹ or in the solid state with, for example, Na for charge compensation and crystal water.⁵² The relatively strong association of this Np^{IV} species with the solid phase ($\log R_d = 4.0$) leaves little doubt about the solid-state nature of this Np^{IV} carbonate species, since the expected 6-fold negative charge of the corresponding pentacarbonate aquo ion would prevent strong sorption to the siderite surface. Furthermore, a fit of the spectrum assuming that Np^{IV} resides in the octahedrally coordinated position of Fe^{II} in siderite failed due to the fact that no Np-C shell at a distance of 3.0–3.4 Å could be fitted, which would be characteristic for the monodentate coordination of carbon in siderite. Therefore, our results demonstrate that Np^{IV} is not entrapped in the siderite structure by coprecipitation, but forms instead a Np^{IV} carbonate precipitate. Evidently, the strong complexation of Np with dissolved carbonate prevented the incorporation by siderite.⁴⁵

ENVIRONMENTAL IMPLICATIONS

After reaction of Np^{V} with siderite in the pH range 7–8 most relevant for siderite-containing clay rocks,⁵⁴ we could demonstrate for the first time the formation of NpO_2 -like nanoparticles. The formation of a NpO_2 -like phase by a surface-mediated redox reaction is in line with results by a recent study showing Np^{V} reduction by biotite and chlorite with reduced structural iron.²⁰ It is also in line with formation of UO_2 -like nanoparticles upon U^{VI} sorption to, for example, magnetite and mackinawite.^{55,56} Formation of monomeric Np^{IV} sorption complexes was not observed at the given reaction conditions, but may form when initial Np concentrations remain below the solubility of $\text{NpO}_2(\text{am})$. Interestingly, the strong affinity of Np^{IV} toward carbonate did not prevent the precipitation of the NpO_2 -like phase, likewise to the formation of PuO_2 after reaction of Pu^{V} with the Fe^{II} hydroxocarbonate chukanovite.¹¹ This can be explained by the relatively low siderite solubility in the investigated pH range. Only during coprecipitation (i.e., when Np^{V} was added to the 0.8 M carbonate solution prior to

siderite precipitation), strong carbonate complexation and subsequent precipitation of a Np^{IV} pentacarbonate took place. Since such high carbonate concentrations are not to be expected under radioactive waste conditions, formation of NpO_2 -like nanoparticles is certainly more relevant for the safety case.

For equilibration periods up to one day, the measured equilibrium concentrations of Np were found to be 2 orders of magnitude larger than those expected in equilibrium with $\text{NpO}_2(\text{am})$ ($[\text{Np}] = 10^{-9} \text{ M}$).⁴⁵ This effect is explained by formation of colloidal $\text{NpO}_2(\text{am})$ in agreement with other amorphous actinide(IV) oxyhydroxide colloids.⁵⁷ After 7 days of equilibration, however, the Np concentrations decreased almost to the value of $\text{NpO}_2(\text{am})$ (SI Table S1). Interestingly, this lower solubility coincides with a higher static order as reflected by lower Debye–Waller factor of the Np-Np paths as compared to the 1 day sample (Table 1). Even addition of a high concentration of carbonate (0.1 M) had only a relatively small influence on Np retention, in line with previous results.^{58,59}

The observed high retention of Np by siderite across a relatively wide pH range is encouraging. However, the potential mobilization of the formed NpO_2 -like nanoparticles as colloids may significantly raise the risk of Np migration away from the waste disposal site.^{60,61} In case of the redox sensitive uranium, the two-electron transition from U^{VI} to U^{IV} requires the formation of a chemical bond with an electron-donor surface, whereas the formation of aqueous Fe-U ion pairs can provide only one electron, thereby hindering the redox reaction kinetically.⁶² Not surprising, TEM images of surface-catalyzed UO_2 show an intimate spatial association with the most reactive sites on mineral surfaces.^{55,56} This is not the case for the NpO_2 particles, which are diffusely distributed between the siderite particles (Figure 3 a), thereby suggesting that the single electron required for the Np^{V} reduction might be provided by dissolved Fe^{II} species. This is further supported by the high isoelectric point of siderite (pH 10.1), leading to charge repulsion between the (net) positively charged siderite surface and the cationic $\text{Np}^{\text{VO}_2^+}$ species prevailing below pH 10, which should also favor the redox reaction between dissolved Np^{V} and Fe^{II} species. Therefore, the NpO_2 -like nanoparticles formed in presence of siderite may have a significant tendency to become detached from the mineral assembly. This does not necessarily mean that they also have a strong tendency to form mobile colloids, since their surface charge is low at circumneutral conditions, which favors their coagulation and causes a relatively fast settling.³⁹ This, however, may change in the presence of dissolved silica, since then amorphous NpO_2 silica structures can form, whose negatively charged silanol surface groups may provide rather stable colloidal suspensions.⁶³

ASSOCIATED CONTENT

Supporting Information

The Supporting Information is available free of charge on the ACS Publications website at DOI: 10.1021/acs.est.6b02399.

Raman spectrum of synthetic siderite; table of XAFS samples; Zeta potential of synthetic siderite; carbonate and Fe solubility in equilibrium with siderite; Np $L_{3\text{-edge}}$ EXAFS fits; HRTEM micrograph and its FFT of 7-d sorption sample after electron irradiation induced changes (PDF)

AUTHOR INFORMATION

Corresponding Author

*Phone: ++33 476 88 2462; e-mail: scheinost@esrf.fr

Notes

The authors declare no competing financial interest.

ACKNOWLEDGMENTS

This work was funded by BMWi (02NUK019D, IMMORAD). We thank the ROBL team, and Maria Berger, Anika Maffert, Christa Müller, Ina Kappler and Sophia Kostudis for their invaluable help. Support by the Ion Beam Center (IBC) at HZDR is gratefully acknowledged. This manuscript greatly benefitted from critical comments by Maria Marques Fernandes (PSI, Switzerland), Xavier Gaona (KIT, Germany) and two anonymous reviewers.

REFERENCES

- Sellin, P.; Leupin, O. X. The use of clay as an engineered barrier in radioactive waste management - A review. *Clays Clay Miner.* **2013**, *61* (6), 477–498.
- Schlegel, M. L.; Bataillon, C.; Blanc, C.; Pret, D.; Foy, E. Anodic activation of iron corrosion in clay media under water-saturated conditions at 90 degrees C: Characterization of the corrosion interface. *Environ. Sci. Technol.* **2010**, *44* (4), 1503–1508.
- Wersin, P.; Jenni, A.; Mader, U. K. Interaction of corroding iron with bentonite in the ABM1 experiment at Aspö, Sweden: A microscopic approach. *Clays Clay Miner.* **2015**, *63* (1–2), 51–68.
- Grambow, B.; Smailos, E.; Geckeis, H.; Müller, R.; Hentschel, H. Sorption and reduction of uranium(VI) on iron corrosion products under reducing saline conditions. *Radiochim. Acta* **1996**, *74*, 149–154.
- El Hajj, H.; Abdelouas, A.; El Mendili, Y.; Karakurt, G.; Grambow, B.; Martin, C. Corrosion of carbon steel under sequential aerobic-anaerobic environmental conditions. *Corros. Sci.* **2013**, *76*, 432–440.
- Marques Fernandes, M.; Ver, N.; Baeyens, B. Predicting the uptake of Cs, Co, Ni, Eu, Th and U on argillaceous rocks using sorption models for Illite. *Appl. Geochem.* **2015**, *59*, 189–199.
- Karland, O. *Chemical and mineralogical characterization of the bentonite buffer for the acceptance control procedure in a KBS-3 repository*; Technical Report SKB TR-10–60: 2010.
- Myneni, S. C. B.; Tokunaga, T. K.; Brown, G. E. Abiotic selenium redox transformations in the presence of Fe(II,III) oxides. *Science* **1997**, *278*, 1106–1109.
- Scheinost, A. C.; Charlet, L. Selenite reduction by mackinawite, magnetite and siderite: XAS characterization of nanosized redox products. *Environ. Sci. Technol.* **2008**, *42* (6), 1984–1989.
- Jaisi, D. P.; Dong, H.; Plymale, A. E.; Fredrickson, J. K.; Zachara, J. M.; Heald, S.; Liu, C. Reduction and long-term immobilization of technetium by Fe(II) associated with clay mineral nontronite. *Chem. Geol.* **2009**, *264* (1–4), 127–138.
- Kirsch, R.; Fellhauer, D.; Altmaier, M.; Neck, V.; Rossberg, A.; Fanghänel, T.; Charlet, L.; Scheinost, A. C. Oxidation state and local structure of plutonium reacted with magnetite, mackinawite and chukanovite. *Environ. Sci. Technol.* **2011**, *45* (17), 7267–7274.
- Um, W.; Chang, H.-S.; Icenhower, J. P.; Lukens, W. W.; Serne, R. J.; Qafoku, N. P.; Westsik, J. H., Jr.; Buck, E. C.; Smith, S. C. Immobilization of 99-Techneium (VII) by Fe(II)-Goethite and Limited Reoxidation. *Environ. Sci. Technol.* **2011**, *45* (11), 4904–4913.
- Huber, F.; Schild, D.; Vitova, T.; Rothe, J.; Kirsch, R.; Schafer, T. U(VI) removal kinetics in presence of synthetic magnetite nanoparticles. *Geochim. Cosmochim. Acta* **2012**, *96*, 154–173.
- Peretyazhko, T. S.; Zachara, J. M.; Kukkadapu, R. K.; Heald, S. M.; Kutnyakov, I. V.; Resch, C. T.; Arey, B. W.; Wang, C. M.; Kovarik, L.; Phillips, J. L.; Moore, D. A. Pertechetate (TcO₄⁻) reduction by reactive ferrous iron forms in naturally anoxic, redox transition zone sediments from the Hanford Site, USA. *Geochim. Cosmochim. Acta* **2012**, *92*, 48–66.
- Nakata, K.; Nagasaki, S.; Tanaka, S.; Sakamoto, Y.; Tanaka, T.; Ogawa, H. Sorption and reduction of neptunium(V) on the surface of iron oxides. *Radiochim. Acta* **2002**, *90* (9–11), 665–669.
- Nakata, K.; Nagasaki, S.; Tanaka, S.; Sakamoto, Y.; Tanaka, T.; Ogawa, H. Reduction rate of neptunium(V) in heterogeneous solution with magnetite. *Radiochim. Acta* **2004**, *92* (3), 145–149.
- Moyes, L. N.; Jones, M. J.; Reed, W. A.; Livens, F. R.; Charnock, J. M.; Mosselmans, J. F. W.; Hennig, C.; Vaughan, D. J.; Patrick, R. A. D. An X-ray absorption spectroscopy study of neptunium(V) reactions with mackinawite (FeS). *Environ. Sci. Technol.* **2002**, *36* (2), 179–183.
- Christiansen, B. C.; Geckeis, H.; Marquardt, C. M.; Bauer, A.; Roemer, J.; Wiss, T.; Schild, D.; Stipp, S. L. S. Neptunyl (NpO₂⁺) interaction with green rust, GR(Na₂SO₄). *Geochim. Cosmochim. Acta* **2011**, *75* (5), 1216–1226.
- Frohlich, D. R.; Amayri, S.; Drebert, J.; Grolimund, D.; Huth, J.; Kaplan, U.; Krause, J.; Reich, T. Speciation of Np(V) uptake by Opalinus Clay using synchrotron microbeam techniques. *Anal. Bioanal. Chem.* **2012**, *404* (8), 2151–2162.
- Brookshaw, D. R.; Patrick, R. A. D.; Bots, P.; Law, G. T. W.; Lloyd, J. R.; Mosselmans, J. F. W.; Vaughan, D. J.; Dardenne, K.; Morrie, K. Redox Interactions of Tc(VII), U(VI), and Np(V) with Microbially Reduced Biotite and Chlorite. *Environ. Sci. Technol.* **2015**, *49* (22), 13139–13148.
- Wylie, E. M.; Olive, D. T.; Powell, B. A. Effects of Titanium Doping in Titanomagnetite on Neptunium Sorption and Speciation. *Environ. Sci. Technol.* **2016**, *50* (4), 1853–1858.
- O'Loughlin, E. J.; Kelly, S. D.; Kemner, K. M. XAFS Investigation of the Interactions of U-VI with Secondary Mineralization Products from the Bioreduction of Fe-III Oxides. *Environ. Sci. Technol.* **2010**, *44* (5), 1656–1661.
- Ithurbide, A.; Peulon, S.; Miserque, F.; Beaucaire, C.; Chausse, A. Interaction between uranium(VI) and siderite (FeCO₃) surfaces in carbonate solutions. *Radiochim. Acta* **2009**, *97* (3), 177–180.
- Scheinost, A. C.; Kirsch, R.; Banerjee, D.; Fernandez-Martinez, A.; Zaenker, H.; Funke, H.; Charlet, L. X-ray absorption and photoelectron spectroscopy investigation of selenite reduction by Fe(II)-bearing minerals. *J. Contam. Hydrol.* **2008**, *102* (3–4), 228–245.
- McBeth, J. M.; Lloyd, J. R.; Law, G. T. W.; Livens, F. R.; Burke, I. T.; Morris, K. Redox interactions of technetium with iron-bearing minerals. *Mineral. Mag.* **2011**, *75* (4), 2419–2430.
- Scheinost, A. C.; Kirsch, R.; Banerjee, D.; Fernandez-Martinez, A.; Zaenker, H.; Funke, H.; Charlet, L. X-ray absorption and photoelectron spectroscopy investigation of selenite reduction by Fe(II)-bearing minerals. *J. Contam. Hydrol.* **2008**, *102*, 228–245.
- Felmy, A. R.; Rai, D.; Mason, M. J. The solubility of hydrous thorium(IV) oxide in chloride media - Development of an aqueous ion-interaction model. *Radiochim. Acta* **1991**, *55* (4), 177–185.
- Charlet, L.; Wersin, P.; Stumm, W. Surface-charge of MnCO₃ and FeCO₃. *Geochim. Cosmochim. Acta* **1990**, *54* (8), 2329–2336.
- Postma, D. Pyrite and siderite oxidation in swamp sediments. *J. Soil Sci.* **1983**, *34* (1), 163–182.
- Scheinost, A. C.; Schwertmann, U. Color identification of iron oxides and hydroxysulfates - Use and limitations. *Soil Science Society of America Journal* **1999**, *63*, 1463–1471.
- Ikeda-Ohno, A.; Hennig, C.; Rossberg, A.; Funke, H.; Scheinost, A. C.; Bernhard, G.; Yaita, T. Electrochemical and complexation behavior of neptunium in aqueous perchlorate and nitrate solutions. *Inorg. Chem.* **2008**, *47* (18), 8294–8305.
- Bruno, J.; Wersin, P.; Stumm, W. On the influence of carbonate in mineral dissolution. 2. The solubility of FeCO₃(s) at 25-degrees-C and 1 atm total pressure. *Geochim. Cosmochim. Acta* **1992**, *56* (3), 1149–1155.
- Webb, S. M. SIXpack: a graphical user interface for XAS analysis using IFEFFIT. *Phys. Scr.* **2005**, *T115*, 1011–1014.
- Ressler, T. WinXAS: a program for X-ray absorption spectroscopy data analysis under MS-Windows. *J. Synchrotron Radiat.* **1998**, *5*, 118–122.

- (35) Ankudinov, A. L.; Rehr, J. J. Relativistic calculations of spin-dependent x-ray-absorption spectra. *Phys. Rev. B: Condens. Matter Mater. Phys.* **1997**, *56*, 1712–1728.
- (36) Benedict, U.; Dabos, S.; Dufour, C.; Spirlet, J. C.; Pages, M. Neptunium compounds under high pressure. *J. Less-Common Met.* **1986**, *121*, 461–468.
- (37) Effenberger, H.; Mereiter, K.; Zemann, J. Crystal-structure refinements of magnesite, calcite, rhodochrosite, siderite, smithonite, and dolomite, with discussion of some aspects of the stereochemistry of calcite-type minerals. *Z. Kristallogr. - Cryst. Mater.* **1981**, *156* (3–4), 233–243.
- (38) Hennig, C. Evidence for double-electron excitations in the L_{3-} edge x-ray absorption spectra of actinides. *Phys. Rev. B: Condens. Matter Mater. Phys.* **2007**, *75* (035120), 035120–1–035120–7.
- (39) Husar, R.; Hübner, R.; Hennig, C.; Martin, P. M.; Chollet, M.; Weiss, S.; Stumpf, T.; Zänker, H.; Ikeda-Ohno, A. Intrinsic formation of nanocrystalline neptunium dioxide under neutral aqueous conditions relevant to deep geological repositories. *Chem. Commun.* **2015**, *51* (7), 1301–1304.
- (40) Rossberg, A.; Scheinost, A. C.; Schmeisser, N.; Rothe, J.; Kaden, P.; Schild, D.; Wiss, T.; Daehn, R. AcReDaS, an Actinide Reference Database for XAS, EELS, IR, Raman and NMR Spectroscopy. In <http://www.hzdr.de/acredas>, 2014.
- (41) Zavarin, M.; Roberts, S. K.; Hakem, N.; Sawvel, A. M.; Kersting, A. B. Eu(III), Sm(III), Np(V), Pu(V), and Pu(IV) sorption to calcite. *Radiochim. Acta* **2005**, *93* (2), 93–102.
- (42) Tits, J.; Wieland, E.; Bradbury, M. H.; Eckert, P.; Schaible, A. *The Uptake of Eu(III) and Th(IV) by Calcite under Hyperalkaline Conditions*; PSI Bericht Nr. 02–03; Villigen, Switzerland, 2002.
- (43) Rossberg, A.; Reich, T.; Bernhard, G. Complexation of uranium(VI) with protocatechuic acid - application of iterative transformation factor analysis to EXAFS spectroscopy. *Anal. Bioanal. Chem.* **2003**, *376* (5), 631–638.
- (44) Lemire, R. J.; Fuger, J.; Nitsche, H.; Potter, P.; Rand, M. H.; Rydberg, J.; Spahiu, K.; Sullivan, J. C.; Ullmann, W. J.; Vitorge, P.; Wanner, H. *Chemical Thermodynamics of Neptunium and Plutonium*. Elsevier: Amsterdam, 2001; p 870.
- (45) Guillaumont, R.; Fanghänel, T.; Fuger, J.; Grenthe, I.; Neck, V.; Palmer, D. A.; Rand, M. H. *Update on the Chemical Thermodynamics of Uranium, Neptunium, Plutonium, Americium and Technetium*; Elsevier: Amsterdam, 2003.
- (46) Funke, H.; Scheinost, A. C.; Chukalina, M. Wavelet analysis of extended X-ray absorption fine structure data. *Phys. Rev. B: Condens. Matter Mater. Phys.* **2005**, *71*, 094110.
- (47) Zachariassen, W. H. Crystal chemical studies of the 5f-series of elements: XII. New compounds representing known structure type. *Acta Crystallogr.* **1949**, *2*, 388–390.
- (48) Rothe, J.; Denecke, M. A.; Neck, V.; Müller, R.; Kim, J. I. XAFS investigation of the structure of aqueous thorium(IV) species, colloids, and solid thorium(IV) oxide/hydroxide. *Inorg. Chem.* **2002**, *41* (2), 249–258.
- (49) Rothe, J.; Walther, C.; Denecke, M. A.; Fanghanel, T. XAFS and LIBD investigation of the formation and structure of colloidal Pu(IV) hydrolysis products. *Inorg. Chem.* **2004**, *43* (15), 4708–4718.
- (50) Ikeda-Ohno, A.; Hennig, C.; Tsushima, S.; Scheinost, A. C.; Bernhard, G.; Yaita, T. Speciation and structural study of U(IV) and -(VI) in perchloric and nitric acid solutions. *Inorg. Chem.* **2009**, *48* (15), 7201–7210.
- (51) Taylor, D. Thermal-expansion data. 2. Binary oxide with the fluorite and rutile structures, MO_2 , and the antiferroite structure, M_2O . *Transactions and Journal of the British Ceramic Society* **1984**, *83* (2), 32–37.
- (52) Hennig, C.; Ikeda-Ohno, A.; Emmerling, F.; Kraus, W.; Bernhard, G. Comparative investigation of the solution species $[U(CO_3)_5]^{6-}$ and the crystal structure of $Na_6[U(CO_3)_5] \cdot 12H_2O$. *Dalton Trans.* **2010**, *39* (15), 3744–3750.
- (53) Clark, D. L.; Conradson, S. D.; Keogh, D. W.; Palmer, P. D.; Scott, B. L.; Tait, C. D. Identification of the limiting species in the plutonium(IV) carbonate system. Solid state and solution molecular structure of the $Pu(CO_3)_5$ (6-) ion. *Inorg. Chem.* **1998**, *37* (12), 2893–2899.
- (54) Baeyens, B.; Thoenen, T.; Bradbury, M. H.; Marques Fernandes, M. *Sorption Data Bases for Argillaceous Rocks and Bentonite for the Provisional Safety Analysis for SGT-E2*; Nagra: Wettingen, Switzerland, 2014.
- (55) Latta, D. E.; Gorski, C. A.; Boyanov, M. I.; O'Loughlin, E. J.; Kemner, K. M.; Scherer, M. M. Influence of Magnetite Stoichiometry on U-VI Reduction. *Environ. Sci. Technol.* **2012**, *46* (2), 778–786.
- (56) Veeramani, H.; Scheinost, A. C.; Monsegue, N.; Qafoku, N. P.; Kukkadapu, R.; Newville, M.; Lanzirotti, A.; Pruden, A.; Murayama, M.; Hochella, M. F., Jr. Abiotic reductive immobilization of U(VI) by neptunium mackinawite. *Environ. Sci. Technol.* **2013**, *47*, 2361–2369.
- (57) Zänker, H.; Hennig, C. Colloid-borne forms of tetravalent actinides: A brief review. *J. Contam. Hydrol.* **2014**, *157*, 87–105.
- (58) Kim, B. Y.; Oh, J. Y.; Baik, M. H.; Yun, J. I. Effect of carbonate on the solubility of neptunium in natural granitic groundwater. *Nucl. Eng. Technol.* **2010**, *42* (5), 552–561.
- (59) Kitamura, A.; Kohara, Y. Carbonate complexation of neptunium(IV) in highly basic solutions. *Radiochim. Acta* **2004**, *92* (9–11), 583–588.
- (60) Walther, C.; Denecke, M. A. Actinide Colloids and Particles of Environmental Concern. *Chem. Rev.* **2013**, *113* (2), 995–1015.
- (61) Kersting, A. B. Plutonium Transport in the Environment. *Inorg. Chem.* **2013**, *52* (7), 3533–3546.
- (62) Liger, E.; Charlet, L.; Van Cappellen, P. Surface catalysis of uranium(VI) reduction by iron(II). *Geochim. Cosmochim. Acta* **1999**, *63* (19/20), 2939–2955.
- (63) Husar, R.; Weiss, S.; Hennig, C.; Hübner, R.; Ikeda-Ohno, A.; Zänker, H. Formation of neptunium(IV)-silica colloids at near-neutral and slightly alkaline pH. *Environ. Sci. Technol.* **2015**, *49*, 665–671.